Pharmacogn. Res., 2027; 19(1):356-369.
https://www.phcogres.com

Original Article

Shenmai Injection Attenuates Pressure Overload-Induced Cardiac Hypertrophy by Modulating HRAS

Xiaojuan Zhou[1,#], Xueying Xu[2,#], Xiaolu Hou[2], Mulan Wang[3], Tian Liang[4], Peiqiang Shen[3,2], Shujing Zhang[5,2], Han Wang[6], Yingchao Wang[2,5], Qinqin Zhao[1,*]

[1]Department of Pharmacy, Tongde Hospital of Zhejiang Province, Hangzhou, CHINA.
[2]Pharmaceutical Informatics Institute, School of Pharmacy, Zhejiang University, Hangzhou, CHINA.
[3]Department of Medicine, Chiatai Qingchunbao Pharmaceutical Co., Ltd., Hangzhou, CHINA.
[4]Department of Cardiology, The Second Affiliated Hospital, School of Medicine, Zhejiang University, Hangzhou, CHINA.
[5]Department of Traditional Chinese Medicine, Innovation Institute for Artificial Intelligence in Medicine, Zhejiang University, Hangzhou, CHINA.
[6]School of Chemistry and Chemical Engineering, Shanghai University of Engineering Science, Shanghai, CHINA.
[#]*These authors contributed equally to this work and are co-first authors.*

ABSTRACT

Background/Objectives: Pressure overload-induced cardiac hypertrophy is a critical pathological precursor in the development of heart failure. Shenmai Injection (SMI) is widely used to treat cardiovascular diseases. However, its anti-hypertrophic effects and underlying molecular mechanisms remain insufficiently elucidated. **Materials and Methods:** Network pharmacology, molecular docking, and experimental validation were systematically utilized. Firstly, active ingredients of SMI were screened using the SwissADME database, and their potential targets were predicted using SwissTargetPrediction. Hypertrophic Cardiomyopathy (HCM)-related targets were retrieved from the GeneCards, OMIM, and DrugBank databases. Protein-Protein Interaction (PPI) networks were optimized using CytoNCA and MCODE plugins, and binding affinities were validated via CB-DOCK. SMI's therapeutic efficacy was validated both *in vitro* and *in vivo* experiments. **Results:** Network pharmacology analysis indicated that the active ingredients of SMI were predominantly enriched in the PI3K-Akt, MAPK, and Ras signaling pathways, with HRAS, SRC, and PRKCA identified as core targets. Molecular docking confirmed a high binding affinity between Methylophiopogonanone B and HRAS. Phalloidin staining demonstrated that SMI dose-dependently inhibited PE-induced hypertrophy in primary neonatal rat cardiomyocytes. TAC successfully induced cardiac hypertrophy in mice, evidenced by increased heart weight-to-body weight ratio, ventricular wall thickening (IVSd, LVPWd), elevated LVSP and LVEDP, and marked myocardial fibrosis. SMI intervention significantly ameliorated the hypertrophic phenotype, reversed hemodynamic parameters, mitigated fibrosis, and down-regulated the overexpressed HRAS. **Conclusion:** SMI exerts anti-hypertrophic and anti-fibrotic effects by downregulating HRAS expression and subsequently inhibiting downstream hypertrophic signaling cascades, thereby effectively ameliorating pressure overload-induced ventricular remodeling.

Keywords: Cardiac Hypertrophy, HRAS, Network Pharmacology, Shenmai Injection.

Correspondence:
Qinqin Zhao
Department of Pharmacy, Tongde Hospital of Zhejiang Province, Hangzhou-310012, CHINA.
Email: qinqin180@126.com

Received: 21-06-2026;
Revised: 19-08-2026;
Accepted: 04-09-2026.

INTRODUCTION

The maintenance of cardiac homeostasis relies on a delicate balance between structural integrity and hemodynamic demand. Under chronic pressure overload, the heart undergoes a sophisticated transition known as cardiac remodeling, of which myocardial hypertrophy is the hallmark early feature (Nakamura and Sadoshima, 2018). While initially serving as a compensatory mechanism to normalize wall stress, sustained biomechanical stretching triggers a detrimental cascade of events, including the reactivation of fetal gene programs and the excessive deposition of extracellular matrix (Oldfield *et al.*, 2020; Shi and Jiang, 2022). This pathological expansion of both cellular and fibrotic compartments leads to increased myocardial stiffness and diastolic dysfunction, eventually reaching a "point of no return" that culminates in terminal heart failure and sudden cardiac death (Schuetze *et al.*, 2014).

Despite the clinical prevalence of neurohumoral inhibitors, such as ACEIs and β-blockers, the "residual risk" of adverse cardiac remodeling remains significant. Consequently, there is a shifting paradigm toward identifying multi-dimensional pharmacological agents that can simultaneously orchestrate systemic responses

DOI: 10.5530/pres.20270208

across the complex landscape of cardiomyocyte growth and interstitial fibrosis.

Shenmai Injection (SMI), a standardized botanical formula derived from *Panax ginseng* and *Ophiopogon japonicus*, has been clinically utilized for decades to stabilize hemodynamic status and support myocardial function in cardiovascular diseases (Li *et al*., 2011). Emerging evidence suggests that SMI exerts its cardioprotective effects through a multi-target synergy, particularly in modulating oxidative stress and suppressing pathological gene programs (Lu *et al*., 2024; Zhao *et al*., 2018). However, the precise molecular interactome through which SMI orchestrates the crosstalk between pro-hypertrophic kinases and fibrotic effectors remains a critical knowledge gap.

Among the intricate signaling networks driving this maladaptive process, HRAS, a critical upstream small GTPase, functions as a master molecular switch translating biomechanical stress into intracellular hypertrophic kinase cascades (such as the MAPK/ERK pathway) (Kubin *et al*., 2020; Matsuda *et al*., 2017; Ramos-Kuri *et al*., 2021). Given its central role in initiating cardiac remodeling, we hypothesized that the multi-component synergy of SMI exerts its anti-hypertrophic efficacy by directly targeting the HRAS signaling axis. To address this, the present study integrates network pharmacology, molecular docking, and multi-level experimental validation to comprehensively investigate the anti-remodeling effect and mechanisms of SMI. Our findings aim to elucidate the HRAS-dependent network targeted by SMI, providing a robust mechanistic basis for its application in intercepting the progression of cardiac remodeling and preserving ventricular architecture.

MATERIALS AND METHODS

Reagent

Shenmai Injection (Chiatai Qingchunbao Pharmaceutical Co., Ltd., Hangzhou, China), 2,2,2-Tribromoethanol (Sigma-Aldrich, USA), Paraformaldehyde Fix Solution (Sangon Biotech (Shanghai) Co., Ltd., China), Wheat Germ Agglutinin (Sigma-Aldrich, USA), Sirius Red (Solarbio, Beijing, China), Masson's Trichrome Stain Kit (Solarbio, Beijing, China), HRAS Rabbit Polyclonal Antibody (Beyotime, Shanghai, China), (R)-(-)-Phenylephrine hydrochloride (Aladdin, Shanghai, China), Alexa Fluor® 488 Phalloidin (Cell Signaling technology, USA), DAPI Staining Solution (Beyotime, Shanghai, China), Hoechst 33258 DAPI Staining Solution (Beyotime, Shanghai, China), Ultrasensitive ECL chemiluminescence kit (Biosharp, Anhui, China), 180 kDa Prestained Protein Marker (Vazyme, Nanjing, China), GAPDH Rabbit Monoclonal Antibody (Beyotime, Shanghai, China), HRP-labeled Goat Anti-Rabbit IgG(H+L) (Beyotime, Shanghai, China), Western Primary Antibody Dilution Buffer (Beyotime, Shanghai, China), PAGE Gel Quick Preparation Kit (VtuoBio, Hangzhou, China), QuickBlock™ Western Blocking Buffer (Beyotime, Shanghai, China), Restore™ PLUS Western Blot Stripping Buffer (Thermo Fisher Scientific, USA), Neonatal Heart Dissociation Kit (MACS, Germany), DMEM (Dulbecco's modified Eagle's Medium, WISENT), Fetal bovine serum (Corning, USA), Penicillin Streptomycin (Gibco, USA), Thiazolyl blue tetrazolium bromide (Sigma-Aldrich, Germany).

Instruments

ALC-V8S Ventilator (Shanghai Alcott Biotech Co., Ltd., China), Vevo 2100 Imaging System (Visualsonics, Canada); PowerLab Data Acquisition System (ADInstruments, Australia), ImageXpress Micro Confocal High-Content Imaging System (Molecular Devices, USA), ChemiDocTM Imaging System (Bio-Rad, USA), ViiATM 7 Real-Time PCR System (Thermo Fisher Scientific, USA), Fluorescence microscope (Leica, Germany), Microplate reader (TECAN, Switzerland), NanoDrop 2000 (Thermo Fisher Scientific, USA), Pressure Catheters (Millar, USA).

Animals

Specific-pathogen-free male C57BL/6J mice aged 4-6 weeks were purchased from Shanghai SLAC Laboratory Animal Co., Ltd., (Shanghai, China, Certificate No.: SCXK [Hu] 2022-0004). The animals were housed in an air-conditioned room with standard temperature (25°C±1°C) and humidity (45%±5% relative humidity), under a 12-hr light/dark cycle, with free access to water and food. All animal studies were performed following the Guide for the Care and Use of Laboratory Animals (8th ed., 2011) and were approved by the Experimental Animal Ethics Committee of Zhejiang Academy of Traditional Chinese Medicine (Approval No. [2026]005).

Methods

Network Pharmacology Analysis

Collection of Chemical Constituents of SMI

The exact botanical composition of Shenmai Injection (SMI), comprising *Panax ginseng* and *Ophiopogon japonicus*, was verified through the official website of Zhengda Qingchunbao Pharmaceutical Co., Ltd., (http://www.cnqcb.com/). The chemical constituents of both herbs were then systematically retrieved from the TCMBank database (https://tcmbank.cn/), and duplicate entries were removed. To standardize the nomenclature of the chemical constituents, the PubChem database (https://pubchem.ncbi.nlm.nih.gov/) was utilized to document their respective PubChem CID, CAS registry numbers, Molecular Formula (MF), and Molecular Weight (MW). Furthermore, the Simplified Molecular-Input Line-Entry System (SMILES) strings of these compounds were programmatically obtained using the Python third-party library, PubChemPy.

Screening of Active Compounds

To evaluate the drug-likeness and oral bioavailability of the acquired chemical constituents, their corresponding SMILES

strings were inputted into the SwissADME database (http://www.swissadme.ch/). The drug-likeness evaluation was based on Lipinski's Rule of Five. A compound was considered to possess favorable drug-likeness if it met at least three of the following criteria: MW ≤500, Moriguchi Octanol-water Partition Coefficient (MlogP) ≤4.5, number of Hydrogen Bond Donors (HBD) ≤5, and number of Hydrogen Bond Acceptors (HBA) ≤10. The oral bioavailability was assessed using Veber's rule, requiring the number of Rotatable Bonds (ROB) to be ≤10 and the Topological Polar Surface Area (TPSA) to be ≤140. Compounds simultaneously satisfying both Lipinski's and Veber's rules were defined as the active compounds of SMI and retained for subsequent analyses.

Target Prediction of Active Compounds

The SMILES strings of the screened active compounds were uploaded to the SwissTargetPrediction database (http://swisstargetprediction.ch/) to predict their potential pharmacological targets. The target species was strictly set to *Homo sapiens*. Based on the principle of molecular similarity, targets with a Probability > 0 were identified as the putative targets of the corresponding active compounds.

Acquisition and Screening of HCM Targets

Disease-related targets were retrieved from the Human Gene Database (GeneCards, https://www.genecards.org/), the Online Mendelian Inheritance in Man database (OMIM, https://www.omim.org/), and the DrugBank database (https://go.drugbank.com/). "Hypertrophic cardiomyopathy" was used as the search keyword, and the target species was limited to *Homo sapiens*. After removing duplicate targets, target names were standardized using the Python third-party library PyUniProt. Subsequently, the intersection between the SMI active compound targets and the HCM-related targets was determined. A Venn diagram visualizing this intersection was generated using the Python library Matplotlib, and the overlapping genes were identified as the potential therapeutic targets of SMI for HCM.

Construction of the Protein-Protein Interaction (PPI) Network

The identified therapeutic targets were input into the STRING database (https://cn.string-db.org/) to retrieve their corresponding STRING IDs. With the species set to *Homo sapiens* and the minimum required interaction score defined as "medium confidence" (0.400), the initial PPI network relationships were obtained and subsequently imported into Cytoscape software. For the first simplification of the network, isolated nodes without any interactions were eliminated.

For the second simplification, the CytoNCA plugin in Cytoscape was employed to perform a topological analysis. Eight topological parameters were calculated: Betweenness Centrality (BC), Closeness Centrality (CC), Degree Centrality (DC), Eigenvector Centrality (EC), Local Average Connectivity-Based Method (LAC), Network Centrality (NC), Subgraph Centrality (SC), and Information Centrality (IC). Only targets with values exceeding the median of all eight topological parameters were retained.

Finally, the MCODE plugin in Cytoscape was utilized to extract densely connected target clusters using default parameters (degree cutoff ≥2, node score cutoff ≥0.2, k-core ≥2, maximum depth=100). The cluster with the highest MCODE score was identified as the core target cluster for SMI for HCM, yielding the final core PPI network.

GO and KEGG Pathway Enrichment Analysis

To elucidate the biological mechanisms, the identified therapeutic targets of SMI against HCM were submitted to the DAVID database (https://david.ncifcrf.gov/) for Gene Ontology (GO) and Kyoto Encyclopedia of Genes and Genomes (KEGG) pathway enrichment analyses. The GO analysis comprehensively evaluated Biological Processes (BP), Cellular Components (CC), and Molecular Functions (MF). Terms and pathways meeting the strict threshold of both p-value<0.05 and False Discovery Rate (FDR) <0.05 were considered statistically significant and retained for functional interpretation.

Molecular Docking Simulation

The three-Dimensional (3D) crystal structures of the key target proteins related to the therapeutic effects of SMI on HCM were retrieved from the RCSB Protein Data Bank (PDB, https://www.

Table 1: Sequences of primers.

Name of Primers	Primer sequence(5′ to 3′)
ANP-F	CACAGATCTGATGGATTTCAAGA
ANP-R	CCTCATCTTCTACCGGCATC
BNP-F	GTCAGTCGTTTGGGCTGTAAC
BNP-R	AGACCCAGGCAGAGTCAGAA
Myh7-F	CGCATCAAGGAGCTCACC
Myh7-R	CTGCAGCCGCAGTAGGTT
Col1A1-F	CATGTTCAGCTTTGTGGACCT
Col1A1-R	GCAGCTGACTTCAGGGATGT
Col3A1-F	TCCCCTGGAATCTGTGAATC
Col3A1-R	TGAGTCGAATTGGGGAGAAT
αSMA-F	CCAGCACCATGAAGATCAAG
αSMA-R	TCCACATCTGCTGGAAGGTA
GAPDH-F	GGCAAGTTCAATGGCACAGT
GAPDH-R	TGGTGAAGACGCCAGTAGACTC
ELN-F	TGGAGCAGGACTTGGAGGT
ELN-R	CCTCCAGCACCATACTTAGCA
FBN1-F	CCTTCCTGTGGCTCCAGAT
FBN1-R	GCTGCCCCCATTCATACA

rcsb.org/) and downloaded in PDB format. Meanwhile, the 3D structures of the active components of SMI were obtained in SDF format from the PubChem database. Fully automated molecular docking between the active components and the target proteins was performed using the CB-DOCK2 web server (http://183.56.231.194:8001/cb-dock2/index.php) to evaluate and validate the results of the network pharmacology screening. Finally, the docking results were visualized using PyMOL software. A binding free energy of less than -6.0 kcal/mol was established as the threshold indicative of potential binding activity.

Effect of SMI on PE-induced cardiomyocyte hypertrophy

Isolation of primary neonatal cardiomyocytes and cell viability assay

1d old neonatal SD rats were used to isolate primary cardiomyocytes using a commercial cardiomyocyte isolation kit through differential adhesion. The cells were cultured in high glucose DMEM medium containing Brdu, and were seeded into 96-well plates at a density of 5000 cells/well. After adhesion for 48 hr in a 37°C incubator with 5% CO_2, different concentrations of SMI were co-incubated with the cardiomyocytes for another 48 hr. Cell viability was measured by MTT staining, and a viability of no less than 90% of the control group was considered as the safe concentration of SMI for further experiment.

Immunofluorescence staining of cardiomyocyte cytoskeleton

Primary cardiomyocytes were seeded into 96-well plates at a density of 5000 cells/well. After 24 hr of adhesion in the 37°C incubator with 5% CO_2, the medium was replaced with high glucose DMEM containing BrdU, and the cells were cultured for another 24 hr. The experiment was divided into Control group, PE group (100 μM), Low SMI group (100 μM PE and 1% SMI), Middle SMI group (100 μM PE and 2% SMI), High SMI group (100 μM PE and 4% SMI). Then all the cells were washed 3 times with PBS, fixed with 4% paraformaldehyde overnight at 4°C. Subsequently, the cells were co-stained with Hoechst and phallodiin staining solution for 15 min at room temperature. After three washes with PBS, images were captured using the imageXpress Micro Confocal High-Content Imaging System, and area of the cells was analyzed.

In vivo evaluation of the anti-hypertrophic effect of SMI

Transverse Aortic Constriction (TAC) model

The Transverse Aortic Constriction (TAC) model was established as previously described (Ma *et al.*, 2019). Briefly, mice were anesthetized by intraperitoneal injection of 1.5% 2, 2, 2-Tribromoethanol, intubated via the trachea, and connected to a small animal ventilator. The ribs were separated at the 4th-5th intercostal space in the left anterior chest area. A 6-0 silk suture was passed around the aortic arch between the brachiocephalic trunk and the left common carotid artery. A 27-gauge needle was placed above the arch, and the suture was tied tightly around both the aorta and the needle. The needle was then quickly removed to achieve aortic arch constriction. After suturing the chest cavity, muscles, and skin, the animals were placed on a heating blanket for recovery. The Sham group underwent the same procedure, except for the ligation of the aortic arch. After recovery, the mice were randomly divided into Sham group, TAC group and SMI group (SMI). The SMI group received intraperitoneal injections of SMI at a dose of 10 mL/kg, once daily for consecutive 28 days, while the Sham and TAC group received the same amount of normal saline.

Echocardiography

Four weeks after TAC surgery, echocardiography was performed using the Vevo 2100 ultrasound system (Visualsonics, Canada). Mice were anesthetized and fixed on the echocardiography platform. M-mode echocardiograms were obtained, and Left Ventricular Posterior Wall Thickness At End-Diastole (LVPWd), Left Ventricular Internal Diameter At End-Diastole (LVIDd), Left Ventricular Internal Diameter At End-Systole (LVIDs), and Interventricular Septal Thickness At End-Diastole (IVSd) were calculated according to the echocardiography.

Hemodynamic measurement

4 weeks after TAC modeling, mice were anesthetized and fixed again, a Millar catheter was inserted retrogradely into the left ventricle via the right common carotid artery. Hemodynamic parameters such as Left Ventricular Systolic Pressure (LVSP), Left Ventricular End-Diastolic Pressure (LVEDP), maximum rate of left ventricular pressure rise (+dp/dt max), and maximum rate of left ventricular pressure decline (-dp/dt max) were determined.

Cardiac Index Measurement

Four weeks after TAC surgery, the cardiac index was measured. Briefly, after the measurement of echocardiography and hemodynamic, mice were euthanized and the whole heart were excised. After washing with pre-cooled PBS, the heart weight was recorded and tibia length of the mice in each group was measured. Cardiac index was calculated as the heart/body weight ratio and heart/tibia length ratio.

Histopathological Experiments

The whole heart was rinsed with PBS and fixed in paraformaldehyde solution for at least 48 hr. After tissue dehydration and paraffin embedding, paraffin heart sections with a thickness of 4 μm were prepared. Paraffin sections were baked at 67°C for 1 hr, followed by deparaffinizing and rehydrating, while Hematoxylin and Eosin (HE) staining, WGA Staining, Sirius red staining, and Masson's trichrome staining were respectively performed according to the

manufacturer's instructions. The stained images were captured using a fluorescence microscope.

RT-qPCR Experiment

After treatment with Shenmai injection for 4 weeks, mouse hearts were isolated and rinsed with cold PBS. 100 mg left ventricle tissue was weighed and the total RNA was extracted according to the Trizol method. The concentration of RNA was measured using Nanodrop 2000, followed by reverse transcription into mRNA. Gene expression of ANP, BNP, MYH7, α-SMA, COL1A1, COL3A1 and Fibronectin were then determined using a ViiA 7 Q-PCR system. The primer sequences are summarized in Table 1. Relative gene expression was calculated using the $2^{-\Delta\Delta Ct}$ method, with GAPDH used as the normalization control. The thermal cycling conditions were as follows: initial denaturation at 95°C for 30 sec, followed by 40 cycles of 95°C for 10 sec and 60°C for 30 sec. A dissociation stage was included to verify amplification specificity.

Western blot

Myocardial tissues harvested 4 weeks post-TAC were washed with cold PBS and snap-frozen in liquid nitrogen. Total proteins were extracted using RIPA lysis buffer supplemented with protease inhibitors and phosphatase inhibitors. The homogenates were centrifuged at 12,000 rpm for 15 min at 4°C, and the supernatants were collected. Protein concentrations were determined using a BCA protein assay kit. 10 μL protein supernatants were separated by 10% SDS-PAGE and transferred onto PVDF membranes. The membranes were blocked with a rapid blocking buffer for 30 min at room temperature, followed by overnight incubation at 4°C with primary antibodies against HRAS (1:1000) and GAPDH (1:2000). After washing three times with PBST, the membranes were incubated with HRP-conjugated secondary antibodies (1:10000) for 1 hr at room temperature. Following three additional PBST washes, the protein bands were visualized using an ECL detection kit and quantified using Image Lab software.

Immunohistochemistry

Four weeks post-surgery, the isolated hearts were washed with cold PBS, fixed in 4% PFA for 48 hr, and embedded in paraffin. The tissue sections were deparaffinized, rehydrated, and subjected to antigen retrieval using a citrate buffer. Endogenous peroxidase activity was blocked by incubating the sections in a 3% H_2O_2 solution for 25 min at room temperature in the dark. After blocking with 3% BSA for 30 min at room temperature, the sections were incubated overnight at 4°C with a primary antibody against HRAS (1:5000). After washing three times with PBS, the sections were incubated with a corresponding secondary antibody (1:200) for 50 min at room temperature. Following another three PBS washes, the immunoreactivity was visualized using a DAB chromogenic kit. The nuclei were counterstained with hematoxylin. Finally, the sections were dehydrated, cleared, and mounted with neutral resin. Images were acquired using a slide scanning microscope. Under the microscope, hematoxylin-stained nuclei appeared blue, while DAB-stained HRAS-positive areas exhibited a brownish-yellow color.

Statistical Analysis

All data are expressed as mean±SEM and were analyzed using GraphPad Prism 9 software. Statistical comparisons among multiple groups were performed using one-way Analysis of Variance (ANOVA), and a p value<0.05 was considered statistically significant.

RESULTS

Network Pharmacology

Active Compounds Screening and Target Prediction of SMI

A total of 114 chemical constituents of Shenmai Injection (SMI) were retrieved from the TCMBank database, comprising 69 from *Panax ginseng* and 45 from *Ophiopogon japonicus*. The ADMET properties of these constituents were subsequently evaluated using the SwissADME database. Based on Lipinski's Rule of Five and Veber's rules, 72 active compounds were initially screened, including 38 from *P. ginseng* and 34 from *O. japonicus*. After excluding 7 compounds that lacked valid putative targets, a final panel of 65 active compounds (34 from *P. ginseng* and 31 from *O. japonicus*) was established.

The potential targets of these active compounds were predicted using the SwissTargetPrediction database, yielding an initial total of 2,786 targets. After eliminating duplicates, 718 unique targets were successfully screened and identified for downstream

Identification of SMI-HCM Intersection Targets

The keyword "Hypertrophic Cardiomyopathy" (HCM) was used to search the GeneCards, OMIM, and DrugBank databases, yielding 227, 404, and 4 disease-related targets, respectively. After removing duplicates, a total of 592 HCM-related targets were identified. By intersecting the putative targets of SMI active compounds with these HCM-related targets, 47 overlapping targets were obtained, representing the potential therapeutic targets of SMI against HCM (Figure 1A).

PPI Network Construction and Core Target Analysis

The 47 intersecting targets were uploaded to the STRING database. Forty-six targets were successfully recognized, while one target was unmatched. Based on the 46 recognized targets, an initial Protein-Protein Interaction (PPI) network was constructed, comprising 46 nodes and 148 edges. After removing four isolated nodes, an initial simplified network of 42 nodes and 148 edges was obtained. Subsequent topological analysis using the CytoNCA plugin yielded a refined network consisting of

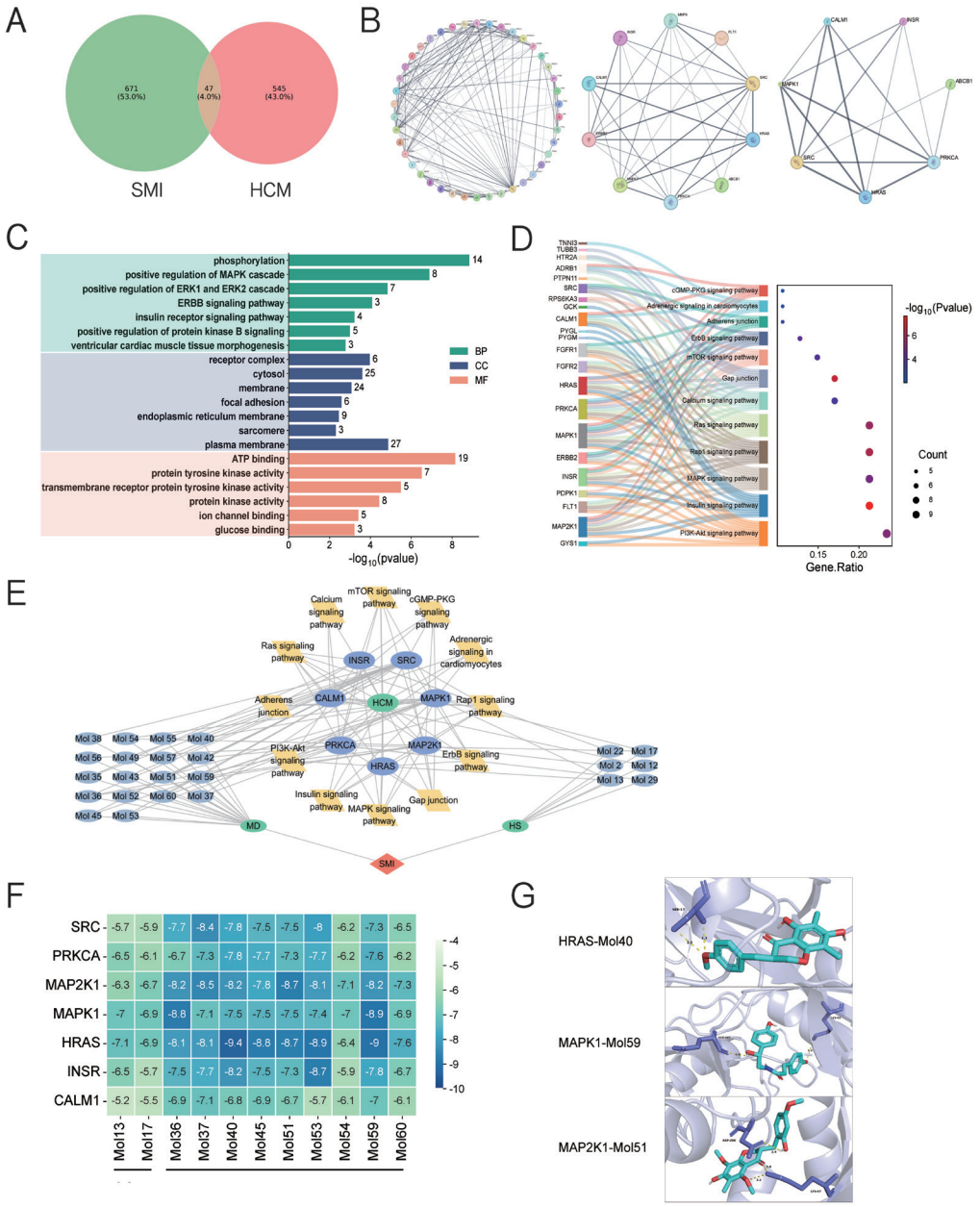

Figure 1: Network pharmacology and molecular docking analysis reveals the potential targets and mechanisms of Shenmai Injection (SMI) against Hypertrophic Cardiomyopathy (HCM). (A) Venn diagram illustrating the overlapping targets between SMI and HCM. (B) Protein-Protein Interaction (PPI) network analysis and topological screening. (C) Gene Ontology (GO) functional enrichment analysis. (D) KEGG signaling pathway enrichment analysis. (E) Construction of the comprehensive "Disease-Drug-Ingredient-Target-Pathway" network. (F) Heatmap of binding energies. (G) Representative 3D molecular docking models.

10 nodes and 32 edges. Finally, analysis via the MCODE plugin identified a core target cluster composed of 7 nodes and 16 edges (score=5.333). In the network visualization, larger node sizes correspond to higher MCODE scores. The three targets with the highest MCODE scores were, HRAS, SRC and PRKCA (Figure 1B). Therefore, it is postulated that SMI primarily acts on HRAS, SRC,PRKCA, ABCB1, CALM1, INSR, and MAPK1 to treat HCM, with HRAS, SRC, and PRKCA serving as the pivotal hub targets.

GO and KEGG Pathway Enrichment Analysis

The 47 therapeutic targets of SMI for HCM were inputted into the DAVID database for Gene Ontology (GO) and Kyoto Encyclopedia of Genes and Genomes (KEGG) pathway enrichment analysis. The GO enrichment analysis (Figure 1C) revealed the multi-target and multi-pathway characteristics of SMI. In terms of Molecular Function (MF), the target genes were significantly enriched in ATP binding, protein tyrosine

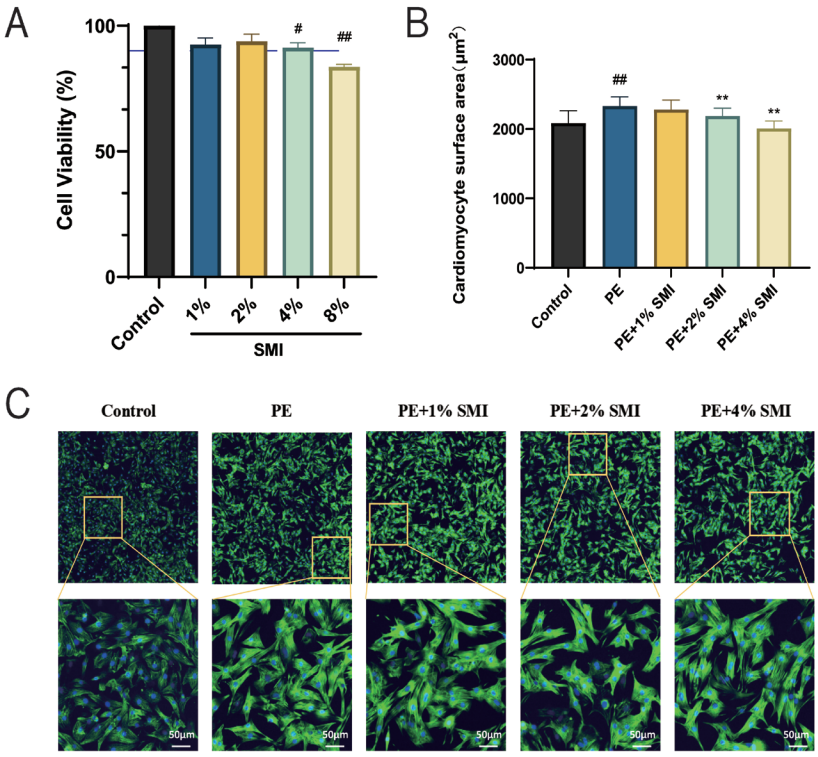

Figure 2: Effects of SMI on PE-induced cardiomyocyte hypertrophy and viability. (A) Cell viability assay. The dashed line indicates 90% cell viability, defined as the threshold for the non-cytotoxic concentration range. (B) Representative immunofluorescence images of cardiomyocytes (scale bar=50 μm). (C) Quantitative analysis of cardiomyocyte surface area. Data are presented as mean±SEM. ## p<0.01, compared with the control group. * p<0.05, ** p<0.01, compared with the PE model group.

kinase activity, and protein kinase activity, indicating a profound kinase inhibitory potential of the active compounds. Regarding Biological Processes (BP), the targets were highly involved in the regulation of phosphorylation, positive regulation of the MAPK cascade, positive regulation of ERK1/2 cascade, and the insulin receptor signaling pathway. This suggests that SMI may exert anti-proliferative, metabolic-regulating, or anti-inflammatory biological effects by modulating classic MAPK/ERK and receptor tyrosine kinase pathways. For Cellular Components (CC), the targets were widely distributed across the plasma membrane, the cytosol, and receptor complex, which aligns perfectly with their roles as signaling pathway modulators.

Furthermore, the KEGG pathway enrichment analysis (Figure 1D) demonstrated that the targets were predominantly enriched in key regulatory networks, including the PI3K-Akt, MAPK, Ras, and insulin signaling pathways. Notably, MAPK1, MAP2K1, HRAS, and INSR emerged as hub genes linking multiple core pathways, thereby participating in the crosstalk between signaling cascades. The highly significant enrichment of the PI3K-Akt and insulin pathways further highlights the specificity of SMI in regulating cellular metabolic homeostasis and growth inhibition.

Herb-Component-Target-Pathway Network

To visualize the systemic therapeutic mechanism of SMI, an integrated "Disease-Drug-Ingredient-Target-Pathway" network was constructed (Figure 1E). The network analysis revealed that key active components of SMI, such as Methylophiopogonanone B (Mol 40) and Ophiopogonanone F (Mol51), exert their effects by targeting core nodes including HRAS, MAP2K1, and MAPK1. This interaction synergistically modulates multiple signaling pathways, notably the MAPK, PI3K-Akt, and Insulin pathways.

Collectively, these findings demonstrate that SMI acts through a multi-target systemic pharmacological mode rather than a single target. By targeting key kinase nodes localized in the plasma membrane and cytosol-SRC, PRKCA, INSR, MAPK1, MAP2K1, HRAS, INSR and CALM1-SMI orchestrates phosphorylation levels and ATP-binding processes within critical signaling cascades, thereby achieving systemic intervention in complex biological processes and maintaining metabolic homeostasis.

Molecular Docking Validation of Core Targets

To evaluate the binding potential between SMI components and HCM-related core targets, molecular docking was performed using 11 representative active components against 7 key targets. The results (Figures 1F, 1G) indicated that the selected active

monomers exhibit robust binding affinities with the core target proteins, with binding free energies predominantly ranging from -7.0 to -9.4 kcal/mol. Notably, HRAS and MAP2K1 exhibited superior sensitivity, specifically, the binding energy between Methylophiopogonanone B (Mol40) and HRAS reached -9.4 kcal/mol, suggesting a high degree of targeted potential. Additionally, MAPK1 demonstrated broad binding versatility, maintaining stable interactions (more negative than -7.0 kcal/mol) with the majority of the tested monomers, which provides a broad foundation for multi-target intervention.

Interaction mode analysis further confirmed that these active components embed into the catalytic pockets of target proteins through stable hydrogen bonding and hydrophobic interactions

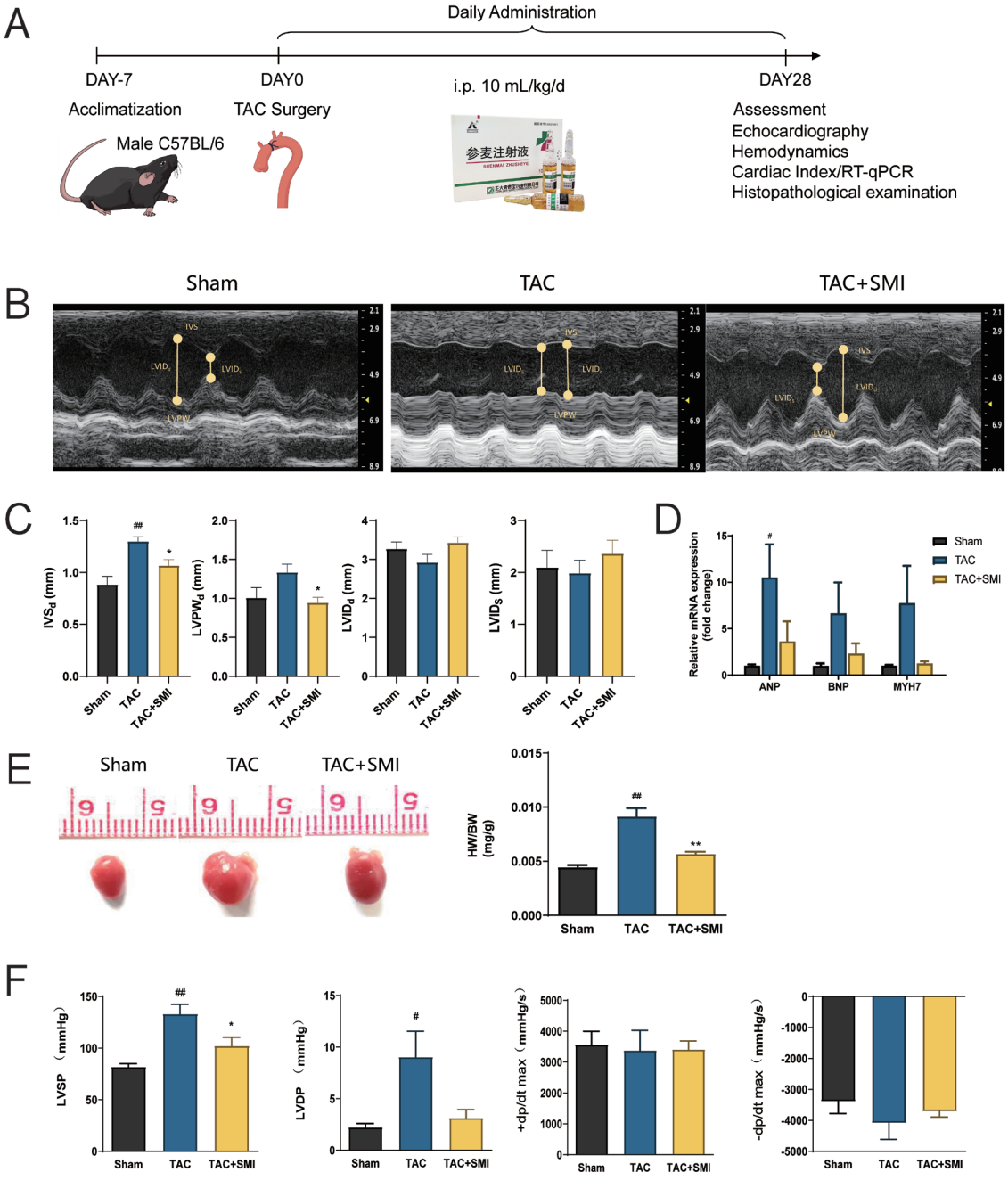

Figure 3: Effects of SMI on cardiac function and morphology in TAC-induced cardiac hypertrophy mice. (A) Schematic representation of the experimental protocol. (B) Representative M-mode echocardiography images of mice from different experimental groups. (C) Statistical analysis of echocardiographic parameters. (D) Relative mRNA expression levels of cardiac hypertrophic genes. (E) Gross cardiac morphology and quantitative analysis of the HW/BW ratio. (F) Hemodynamic assessment. *n*=5-8 mice per group. Data are presented as mean±SEM. # $p<0.05$, ## $p<0.01$, compared with the Sham group. * $p<0.05$, ** $p<0.01$, compared with the TAC model group.

with key amino acid residues. This computational evidence highly aligns with the aforementioned GO and KEGG enrichment results, strongly supporting the molecular hypothesis that SMI attenuates cardiac remodeling by synergistically inhibiting core kinases and subsequently modulating the MAPK and PI3K-Akt signaling networks.

In vitro Experiment

Effect of SMI on the Viability of Primary Neonatal Cardiomyocytes

To ensure that the observed pharmacological effects were not confounded by drug-induced cytotoxicity, we first evaluated the impact of varying concentrations of SMI on the viability of primary neonatal cardiomyocytes (Figure 2A). Defining a safe therapeutic window as maintaining cell viability at ≥90% of the control group, our assays revealed that incubation with 1%, 2% and 4% SMI did not significantly alter cell survival. In contrast, administration of 8% SMI induced substantial cellular toxicity ($p<0.01$). Concentrations of 1%, 2%, and 4% SMI were selected for all subsequent *in vitro* functional assays.

SMI dose-dependently attenuates PE-induced cardiomyocyte hypertrophy

To validate the anti-hypertrophic efficacy of SMI at the cellular level, we established an *in vitro* model of cardiomyocyte hypertrophy using Phenylephrine (PE) stimulation. Cellular morphology was visualized via fluorescence co-staining with phalloidin (cytoskeleton, green) and Hoechst (nuclei, blue) (Figure 2B). Microscopic evaluation revealed that PE exposure induced a classical hypertrophic phenotype, characterized by pronounced cytoskeletal expansion. Quantitative analysis confirmed a statistically significant increase in the total cell surface area in the PE group compared to the control group ($p<0.01$). Strikingly, co-treatment with SMI effectively ameliorated these PE-induced structural abnormalities. Further quantitative assessment demonstrated that SMI intervention restricted the expansion of the cardiomyocyte surface area in a dose-dependent manner, with the 2% and 4% SMI treatment groups exhibiting highly significant reductions compared to the PE-only group ($p<0.01$) (Figure 2C).

In vivo Experiment

SMI ameliorates cardiac structural abnormalities in TAC-induced mice

Echocardiography was employed to evaluate the cardioprotective effects of SMI against pressure overload-induced hypertrophy. Representative echocardiographic images (Figures 3A, 3B) showed that mice in the Sham group exhibited regular ventricular wall motion and normal wall thickness. In contrast, the TAC group displayed significant ventricular wall thickening, a hallmark of concentric hypertrophy induced by pressure overload. Following SMI intervention, the progression of wall thickening was mitigated, and the cardiac structure trended toward normalization. Quantitative analysis of echocardiographic parameters (Figures 3C, 3D) further revealed that both the Interventricular Septum Thickness At End-Diastole (IVSd) and the Left Ventricular Posterior Wall Dimension at End-Diastole (LVPWd) were significantly increased in the TAC group compared to the Sham group ($p<0.01$), confirming concentric ventricular thickening. Administration of SMI significantly improved both IVSd and LVPWd compared to the TAC group ($p<0.05$), effectively suppressing the degree of cardiac hypertrophy. Additionally, the Left Ventricular Internal Diameters At End-Diastole And End-Systole (LVIDd and LVIDs) also showed a favorable trend toward improvement following SMI treatment.

Regulatory effects of SMI on cardiac hemodynamics in TAC-induced mice

Further evaluation of cardiac function and pressure overload was conducted by measuring left ventricular hemodynamic parameters via right carotid artery catheterization at 4 weeks post-surgery (Figure 3F). The results demonstrated that the Left Ventricular Systolic Pressure (LVSP) in the TAC group was significantly elevated compared to the Sham group ($p<0.01$), indicating an increased afterload on the left ventricle. Concurrently, the Left Ventricular End-Diastolic Pressure (LVEDP), a key indicator of ventricular filling pressure and diastolic function, was also significantly upregulated in the TAC group ($p<0.05$), suggesting that pressure overload had induced diastolic restriction. Following 4 weeks of SMI intervention, the LVSP in the SMI-treated group was markedly reduced compared to the model group ($p<0.05$), effectively alleviating the continuous myocardial damage caused by high-pressure load. Furthermore, while no statistically significant differences were observed among groups in terms of the maximum rate of pressure rise ($+dp/dt_{max}$) and fall ($-dp/dt_{max}$), the LVEDP in the SMI-treated group showed a notable trend of returning to normal levels compared to the TAC group. These hemodynamic data demonstrate from a biomechanical perspective that SMI can effectively delay the progression of pressure overload-induced cardiac hypertrophy by reducing the left ventricular pressure load.

SMI reverses TAC-induced changes in gross cardiac morphology and heart weight-to-body weight ratio

The degree of cardiac hypertrophy was assessed by observing the gross morphology of the hearts and calculating the Heart Weight-to-Body Weight (HW/BW) ratio (Figures 3E). Compared to the Sham group, mice in the TAC model group exhibited a significant increase in heart size and a markedly elevated HW/BW ratio at 4 weeks post-surgery ($p<0.01$). After 4 weeks of continuous intraperitoneal administration of SMI, the heart size was noticeably reduced, and the HW/BW ratio was significantly lower than that of the TAC group ($p<0.01$). These findings

indicate that SMI treatment effectively inhibits TAC-induced cardiac hypertrophy in mice.

Effect of SMI on the transcriptional levels of cardiac hypertrophic marker genes in TAC mice

At the molecular level, we employed RT-qPCR to detect the mRNA expression of hypertrophic marker genes in myocardial tissues, providing insights into the inhibitory effect of SMI on cardiac hypertrophy. As shown in Figure 3D, after 4 weeks of TAC induction, the mRNA expression levels of ANP, BNP, and MYH7 were markedly upregulated in the model group. Specifically, the expression of ANP in the TAC group was significantly higher than that in the Sham group ($p<0.05$). Following SMI intervention, the expression of these hypertrophic markers was suppressed to varying degrees, exhibiting a clear trend toward normalization.

SMI ameliorates myocardial tissue morphology and inhibits cardiomyocyte hypertrophy in TAC mice

Histopathological assessments utilizing Hematoxylin and Eosin (H&E) and Wheat Germ Agglutinin (WGA) staining were subsequently performed on heart sections to confirm the protective effects of SMI against cardiac hypertrophy (Figure 4A). H&E staining revealed that the cardiomyocytes in the Sham group were tightly and orderly arranged, presenting normal cellular morphology and structure. In contrast, the TAC model group exhibited marked thickening of the ventricular walls and enlarged cardiomyocyte areas. Consistently, WGA staining, which delineates the cell boundaries, further confirmed that the cross-sectional area of cardiomyocytes in the TAC group was significantly increased compared to that in the Sham group. Following SMI intervention, these pathological changes in the myocardial tissue were significantly ameliorated, and cardiomyocyte hypertrophy was markedly inhibited.

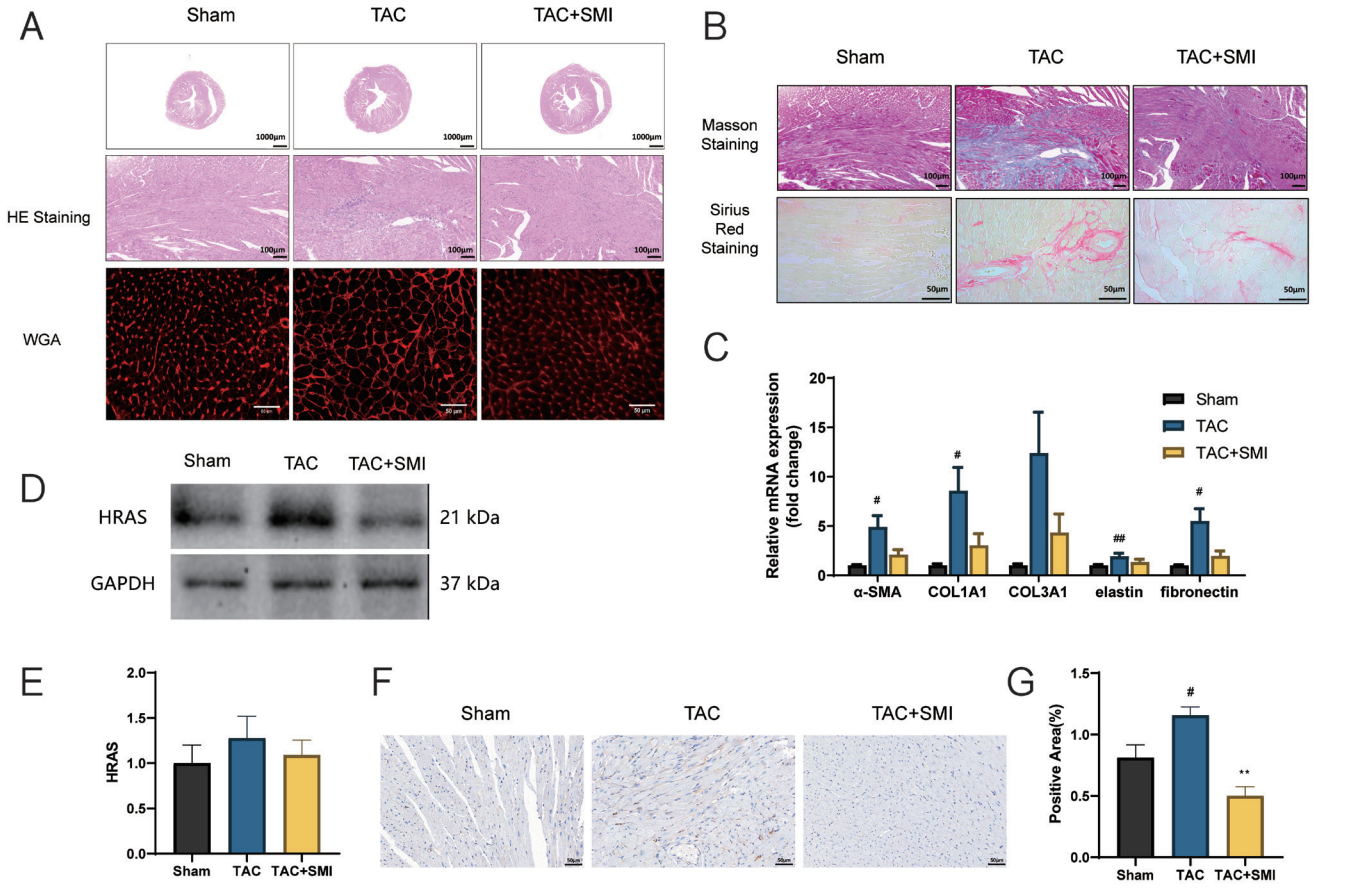

Figure 4: Pathological alterations, myocardial fibrosis, and HRAS protein expression in heart tissues. (A) Representative images of H&E staining (top and middle rows) and WGA staining (bottom row) of heart cross-sections. (B) Representative images of Masson's trichrome staining (top row) and Sirius Red staining (bottom row) of heart tissues. (C) Quantitative analysis of cardiomyocyte cross-sectional area and the percentage of fibrotic area. (D) Representative Western blot images. (E) Quantitative analysis of relative HRAS protein expression levels. (F) Representative IHC staining images. (G) Quantitative analysis of the percentage of HRAS-positive staining. Data are presented as mean±SEM. # $p<0.05$, compared with the Sham group. * $p<0.05$, ** $p<0.01$, compared with the TAC model group.

SMI attenuates TAC-induced myocardial fibrosis and collagen deposition

Myocardial fibrosis and Excessive Extracellular Matrix (ECM) remodeling are critical events in the deterioration of cardiac function induced by pressure overload. We evaluated collagen deposition in the myocardial interstitium using Masson's trichrome staining and Sirius Red staining (Figure 4B). The results showed that the myocardial tissue of the Sham group exhibited only a sparse distribution of collagen fibers. However, in the TAC group, both the blue areas indicating collagen in Masson's staining and the red areas in Sirius Red staining were significantly increased, indicating the occurrence of severe interstitial and perivascular fibrosis. In contrast, the area of collagen staining in the SMI group was markedly reduced compared to the TAC group, suggesting that SMI can effectively attenuate collagen deposition in the myocardial tissue. Furthermore, RT-qPCR was used to detect the transcriptional levels of fibrosis-related genes in the heart tissues (Figure 4C). The results demonstrated that TAC intervention led to a significant upregulation in the mRNA expression of genes associated with fibroblast activation and ECM remodeling (including α-SMA, COL1A1, elastin, and fibronectin) compared to the Sham group ($p<0.05$). Following SMI intervention, the overexpression of these profibrotic marker genes was effectively suppressed, exhibiting a trend of returning toward normal levels. Collectively, these results indicate that SMI significantly antagonizes the progression of TAC-induced myocardial fibrosis.

Western blot validation of the predicted core target HRAS

To evaluate the effect of SMI on the Ras signaling pathway in pressure overload-induced cardiac hypertrophy, we assessed the expression levels of HRAS protein in the myocardial tissues of mice across all experimental groups. Western blot results and subsequent quantitative analysis demonstrated that, compared to the Sham group, HRAS protein expression was upregulated in the myocardium of the TAC group. However, following SMI intervention, the TAC-induced overexpression of HRAS protein was partially attenuated, resulting in a decline in its relative expression levels compared to the TAC group (Figures 4D, 4E). These findings suggest that pressure overload induces the abnormal activation of HRAS in myocardial tissue, and that SMI can partially reverse this process by downregulating HRAS expression. This regulatory effect may represent a potential molecular mechanism underlying the cardioprotective efficacy of SMI against myocardial injury.

Immunohistochemical evaluation of HRAS in TAC-induced mice

To further validate the impact of SMI on HRAS expression at the histological level, Immunohistochemical (IHC) staining was performed on the myocardial tissues of mice from each experimental group. As illustrated in Figure 4F, cell nuclei were counterstained with hematoxylin (blue-purple), while brownish-yellow deposits indicate the positive expression of HRAS protein. Representative microscopic images and quantitative analysis (Figure 4G) revealed that, compared to the Sham group, myocardial tissues in the TAC group exhibited extensive brownish-yellow staining, with a significantly higher percentage of HRAS-positive area ($p<0.05$). Conversely, SMI intervention effectively reduced the HRAS-positive areas in the SMI-treated group. Quantitative assessment confirmed that HRAS expression levels in the SMI-treated group were significantly downregulated compared to the TAC group ($p<0.01$). These morphological findings are highly consistent with the Western blot results, further corroborating that pressure overload induces HRAS protein overexpression in myocardial tissue, a pathological process that can be effectively attenuated by SMI treatment.

Based on the integrated findings from network pharmacology, molecular docking, and *in vivo* experimental validation, we propose a potential mechanism by which SMI ameliorates TAC-induced ventricular remodeling. Specifically, biomechanical stress induced by TAC significantly upregulates HRAS, which serves as a critical upstream node triggering a pathological signaling cascade. SMI, through its core active components, directly targets and downregulates HRAS expression. This targeted inhibition effectively blunts downstream intracellular signaling pathways, yielding a dual therapeutic effect: (1) suppression of cardiomyocyte hypertrophy and reversal of pathological transcriptional reprogramming (ANP, BNP, MYH7); (2) attenuation of extracellular matrix deposition and the expression of pro-fibrotic markers (α-SMA, COL1A1). Ultimately, this synergistic intervention ameliorates structural ventricular remodeling and preserves cardiac hemodynamic stability.

DISCUSSION

The heart possesses high plasticity, allowing it to undergo physiological or pathological hypertrophy depending on the type, intensity, and duration of environmental stimuli. While physiological hypertrophy is typically accompanied by normal or enhanced contractile function and preserved cardiac architecture, pathological hypertrophy is closely associated with cardiomyocyte death and interstitial fibrotic remodeling. The latter is characterized by a progressive decline in systolic and diastolic functions, ultimately culminating in an irreversible progression toward heart failure (Packard *et al.*, 2022; Wang *et al.*, 2025). Mechanical stress and neurohumoral stimulation serve as the primary triggers for cardiac hypertrophy, regulating a variety of cellular responses-including gene expression, protein synthesis, sarcomere assembly, and cellular metabolism-that drive the development and progression of the disease (Shimizu and Minamino, 2016).

Current clinical pharmacological interventions for myocardial hypertrophy primarily include β-blockers, Calcium Channel Blockers (CCBs), Angiotensin Receptor Blockers (ARBs), and statins. Despite their distinct mechanisms and therapeutic advantages (Kannan *et al.*, 2025; Xu *et al.*, 2024), these targeted therapies often only alleviate clinical symptoms and delay disease progression, failing to fundamentally reverse established ventricular structural remodeling. Shenmai Injection (SMI), a classic Chinese medicinal formula with a long history of clinical application, has been demonstrated in multiple clinical trials to alleviate myocardial injury, improve myocardial metabolism and cardiac function, and reduce the incidence of heart failure (Hu *et al.*, 2012; Li *et al.*, 2023; Wu *et al.*, 2023). Given the advantages of multi-target synergistic intervention in complex cardiovascular diseases, this study combined the Transverse Aortic Constriction (TAC) animal model with network pharmacology to systematically elucidate the molecular mechanisms by which SMI reverses myocardial hypertrophy and improves cardiac function.

In the present study, the TAC model successfully replicated the ventricular wall thickening and hemodynamic alterations induced by pressure overload. Sustained biomechanical stress triggered the pathological transition of the heart from compensatory hypertrophy to dilated failure. Both *in vivo* and *in vitro* results systematically demonstrated that SMI effectively blocked this pathological process. Echocardiography and hemodynamic assessments revealed that SMI significantly reduced wall thickness (IVSd and LVPWd) in TAC mice and restored the homeostasis of left ventricular systolic and diastolic pressures. These findings are consistent with the meta-analysis results reported (Wang *et al.*, 2023). Furthermore, several previous clinical trials have also documented that SMI improves left ventricular function and reduces B-type Natriuretic Peptide (BNP) levels in patients with heart failure (Ma *et al.*, 2010; Wang *et al.*, 2020).

Myocardial fibrosis is a hallmark pathological feature in the evolution of myocardial hypertrophy toward end-stage heart failure. Existing research indicates that SMI can inhibit myocardial fibrosis and effectively improve heart failure by regulating inflammatory cytokines and mitochondrial membrane potential (Hu *et al.*, 2023; Yang *et al.*, 2024; Zhang *et al.*, 2019). Histopathological results in this study (HE, WGA, Masson, and Sirius Red staining) clearly demonstrated that SMI significantly inhibited myocardial collagen deposition. At the molecular level, the downregulation of pro-fibrotic markers α-SMA and COL1A1 further underscores SMI's capacity to inhibit the activation of cardiac fibroblasts and stabilize the Extracellular Matrix (ECM).

Beyond structural improvements, the profound regulatory effect of SMI on cardiomyocyte phenotypic switching warrants significant attention. In this study, we observed that mRNA levels of ANP, BNP, and MYH7 were significantly upregulated in myocardial tissue four weeks post-TAC. The recovery of hemodynamic status is essentially linked to SMI's ability to suppress the "fetal gene program." The elevation of ANP and BNP reflects increased ventricular wall tension and compensatory neurohumoral responses (Goetze *et al.*, 2020), while the upregulation of MYH7 suggests a phenotypic switch of Myocardial Contractile Proteins from the adult isoform (α-MHC) to the embryonic isoform (β-MHC) (Hang *et al.*, 2010). Although this switch is initially compensatory, it leads to failure of cardiac contractile dynamics over the long term. SMI markedly downregulated the expression of these genes, suggesting that it not only reduces cell volume at the physical level but also reverses the pathological attributes of cardiomyocytes at the transcriptional level. This "programmed reversal" helps maintain the normal contractile efficiency of myocardial fibers and prevents the heart from crossing the compensatory threshold into irreversible structural decline.

Overactivation of the Renin-Angiotensin System (RAS) and Sympathetic Nervous System (SNS) is considered the core driver of pathological cardiac hypertrophy (Caturano *et al.*, 2022). HRAS plays a pivotal role in this process as a molecular switch, activating classic signaling cascades such as Ras/Raf/MEK/MAPK, which in turn trigger the expression of hypertrophy-related transcription factors (Ramos-Kuri *et al.*, 2021). Using network pharmacology, this study identified 65 active components in SMI clustered on 47 HCM-related targets, with HRAS, SRC, and PRKCA serving as core hub nodes. KEGG pathway enrichment analysis revealed that the targets of these active components were primarily enriched in key regulatory pathways such as the PI3K-Akt, MAPK, and Ras signaling pathways, suggesting that SMI possesses high specificity in regulating cellular metabolic homeostasis and growth inhibition. Molecular docking provided a structural basis for this efficacy, revealing that Methylophiopogonanone B exhibits a remarkably high binding affinity for HRAS (-9.4 kcal/mol), implying its potential to inhibit kinase activity through competitive binding. Western Blot (WB) results showed that SMI treatment partially suppressed the TAC-induced overexpression of HRAS protein, with its relative expression levels decreasing compared to the TAC group. This experimental evidence aligns with our analysis, suggesting that SMI can cut off the transduction pathway from biomechanical stress to intracellular hypertrophic signals by downregulating the expression of the key node protein HRAS. Since the HRAS pathway is also a critical route for inducing myofibroblast transdifferentiation, its inhibition by SMI likely produces a dual effect: directly inhibiting cardiomyocyte hypertrophy and reducing the paracrine secretion of pro-fibrotic factors, while simultaneously blocking collagen synthesis in fibroblasts. This dual regulation of cardiomyocytes and interstitial components effectively reduces myocardial stiffness and improves cardiac diastolic compliance, thereby comprehensively enhancing hemodynamic performance.

CONCLUSION

SMI exerts anti-hypertrophic and anti-fibrotic effects by downregulating HRAS expression and subsequently inhibiting downstream hypertrophic signaling cascades, thereby effectively ameliorating pressure overload-induced ventricular remodeling. Future studies utilizing HRAS knockout or overexpression mouse models are required to further confirm the absolute necessity of HRAS in the therapeutic efficacy of SMI. The specific combination ratios of SMI's active components and their potential synergistic effects require further in-depth deconstruction. Overall, this study not only provides a solid experimental basis for the clinical application of SMI but also offers a novel intervention strategy for targeting HRAS in the treatment of ventricular remodeling.

ABBREVIATIONS

ANP: Atrial Natriuretic Peptide; **BNP:** Brain Natriuretic Peptide; **BP:** Biological Process; **GO-CC:** Cellular Component; **DMEM:** Dulbecco's Modified Eagle's Medium; **GO:** Gene Ontology; **HCM:** Hypertrophic Cardiomyopathy; **HE:** Hematoxylin and Eosin; **HRAS:** Harvey Rat Sarcoma Viral Oncogene Homolog; **IVS:** Interventricular Septal Thickness; **KEGG:** Kyoto Encyclopedia of Genes and Genomes; **LVEDP:** Left Ventricular End-diastolic Pressure; **LVID:** Left Ventricular Internal Diameter; **LVPW:** Left ventricular Posterior Wall Thickness; **LVSP:** Left ventricular Systolic Pressure; **MF:** Molecular Function; **MYH7:** Myosin Heavy Chain 7; **NRCMs:** Neonatal Rat Cardiomyocytes; **PE:** Phenylephrine; **PPI:** Protein-protein Interaction; **SMI:** Shenmai Injection; **TAC:** Transverse Aortic Constriction; **WB:** Western Blot; **WGA:** Wheat Germ Agglutinin; **α-SMA:** Alpha-smooth Muscle Actin; **BC:** Betweenness centrality; **CC:** Closeness centrality; **DC:** Degree centrality; **EC:** Eigenvector centrality; **LAC:** Local average connectivity-based method; **NC:** Network centrality; **SC:** Subgraph centrality; **IC:** Information centrality; **MW:** Molecular weight; **HBD:** Hydrogen bond donors; **HBA:** Hydrogen bond acceptors; **ROB:** Rotatable bonds; **TPSA:** Topological polar surface area; **MlogP:** Moriguchi octanol-water partition coefficient.

CONFLICT OF INTEREST

The authors declare that there is no conflict of interest.

FUNDING

This study was financially supported by the Traditional Chinese Medicine Science and Technology Project of Zhejiang Province (2024ZL343, X.Z.), the "Pioneer" and "Leading Goose"R&D Program of Zhejiang (2026C02A1078, S.Z.; 2025C01110, Y.W.), and the Zhejiang Medical Association Clinical Research Fund (2023ZYC-A121, X.Z.).

AUTHORS CONTRIBUTION

Research concept and design, X.Z., X.X., X.H., Q.Z.; Collection and/or assembly of data, X.Z., X.X., X.H., M.W., P.S., S.Z. and Y.W.; Data analysis and interpretation, X.X., X.H. and T.L.; Writing the article, X.Z., X.X.; Critical revision of the article, X.Z., H.W., Q.Z. and Y.W.; Final approval of the article, X.Z., Y.W. and Q.Z. All authors have read and agreed to the published version of the manuscript.

SUMMARY

This study integrated network pharmacology, molecular docking, and experimental validation to systematically elucidate the therapeutic effects and mechanisms of Shenmai Injection in pressure overload-induced cardiac hypertrophy. HRAS was identified and validated as a key target mediating the protective effects, providing a novel intervention strategy for the treatment of ventricular remodeling.

REFERENCES

Caturano, A., Vetrano, E., Galiero, R., Salvatore, T., Docimo, G., Epifani, R., Alfano, M., Sardu, C., Marfella, R., Rinaldi, L., & Sasso, F. C. (2022). Cardiac hypertrophy: From pathophysiological mechanisms to heart failure development. Reviews in Cardiovascular Medicine, 23(5), 165. https://doi.org/10.31083/j.rcm2305165

Goetze, J. P., Bruneau, B. G., Ramos, H. R., Ogawa, T., de Bold, M. K., & de Bold, A. J. (2020). Cardiac natriuretic peptides. Nature Reviews Cardiology, 17(11), 698–717. https://doi.org/10.1038/s41569-020-0381-0

Hang, C. T., Yang, J., Han, P., Cheng, H. L., Shang, C., Ashley, E., Zhou, B., & Chang, C. P. (2010). Chromatin regulation by Brg1 underlies heart muscle development and disease. Nature, 466(7302), 62–67. https://doi.org/10.1038/nature09130

Hu, J., Zhang, W., Xie, Y. M., Wang, L. X., Nie, X. L., & Zhang, Y. L. (2012). Meta-analysis of Shenmai injection treatment for acute myocardial infarction. China Journal of Chinese Materia Medica, 37(18), 2760–2767.

Hu, S. Y., Zhou, Y., Zhong, S. J., Yang, M., Huang, S. M., Li, L., Li, X. C., & Hu, Z. X. (2023). Shenmai injection improves hypertensive heart failure by inhibiting myocardial fibrosis via TGF-β1/Smad pathway regulation. Chinese Journal of Integrative Medicine, 29(2), 119–126. https://doi.org/10.1007/s11655-022-2899-y

Kannan, D., Rajasingh, S., Madasamy, P., & Rajasingh, J. (2025). Cardiac hypertrophy at the crossroads: Mechanistic insights and emerging multimodal therapeutic strategies. European Journal of Pharmacology, 1006, 178179. https://doi.org/10.1016/j.ejphar.2025.178179

Kubin, T., Cetinkaya, A., Kubin, N., Bramlage, P., Sen-Hild, B., Gajawada, P., Akintürk, H., Schönburg, M., Schaper, W., Choi, Y. H., Barancik, M., & Richter, M. (2020). The MEK/ERK module is reprogrammed in remodeling adult cardiomyocytes. International Journal of Molecular Sciences, 21(17). https://doi.org/10.3390/ijms21176348

Li, J. S., Wang, H. F., Li, S. Y., Yu, X. Q., & Wang, Z. W. (2011). Shenmai injection for chronic pulmonary heart disease: A systematic review and meta-analysis. The Journal of Alternative and Complementary Medicine, 17(7), 579–587. https://doi.org/10.1089/acm.2010.0354

Li, Y., Fan, L., Wang, X., & Lv, S. (2023). Shenmai injection ameliorates doxorubicin-induced myocardial injury by suppressing autophagy-apoptosis via miR-30a. Aging (Albany NY), 15(21), 12400–12412. https://doi.org/10.18632/aging.205188

Lu, M., Zhang, Y., Ma, X., Cen, M., Lin, S., Qian, X., Yu, J., Huang, X., & Jiang, Z. (2024). Shenmai injection alleviates myocardial ferroptosis via activating the AKT1/mTOR pathway in rats with acute myocardial infarction. Annals of Clinical and Laboratory Science, 54(1), 35–46.

Ma, H., Yu, S., Liu, X., Zhang, Y., Fakadej, T., Liu, Z., Yin, C., Shen, W., Locasale, J. W., Taylor, J. M., Qian, L., & Liu, J. (2019). Lin28a regulates pathological cardiac hypertrophic growth through Pck2-mediated enhancement of anabolic synthesis. Circulation, 139(14), 1725–1740. https://doi.org/10.1161/circulationaha.118.037803

Ma, R. G., Wang, C. X., Shen, Y. H., Wang, Z. Q., Ma, J. H., & Huang, L. S. (2010). Effect of Shenmai injection on ventricular diastolic function in patients with chronic heart failure: An assessment by tissue Doppler imaging. Chinese Journal of Integrative Medicine, 16(2), 173–175. https://doi.org/10.1007/s11655-010-0173-1

Matsuda, T., Jeong, J. I., Ikeda, S., Yamamoto, T., Gao, S., Babu, G. J., Zhai, P., & Del Re, D. P. (2017). H-Ras isoform mediates protection against pressure overload-induced cardiac

dysfunction in part through activation of AKT. Circulation: Heart Failure, 10(2). https://doi.org/10.1161/circheartfailure.116.003658

Nakamura, M., & Sadoshima, J. (2018). Mechanisms of physiological and pathological cardiac hypertrophy. Nature Reviews Cardiology, 15(7), 387–407. https://doi.org/10.1038/s41569-018-0007-y

Oldfield, C. J., Duhamel, T. A., & Dhalla, N. S. (2020). Mechanisms for the transition from physiological to pathological cardiac hypertrophy. Canadian Journal of Physiology and Pharmacology, 98(2), 74–84. https://doi.org/10.1139/cjpp-2019-0566

Packard, E., de Feria, A., Peshin, S., Reza, N., & Owens, A. T. (2022). Contemporary therapies and future directions in the management of hypertrophic cardiomyopathy. Cardiology and Therapy, 11(4), 491–507. https://doi.org/10.1007/s40119-022-00283-5

Ramos-Kuri, M., Meka, S. H., Salamanca-Buentello, F., Hajjar, R. J., Lipskaia, L., & Chemaly, E. R. (2021). Molecules linked to Ras signaling as therapeutic targets in cardiac pathologies. Biological Research, 54(1), 23. https://doi.org/10.1186/s40659-021-00342-6

Schuetze, K. B., McKinsey, T. A., & Long, C. S. (2014). Targeting cardiac fibroblasts to treat fibrosis of the heart: Focus on HDACs. Journal of Molecular and Cellular Cardiology, 70, 100–107. https://doi.org/10.1016/j.yjmcc.2014.02.015

Shi, S., & Jiang, P. (2022). Therapeutic potentials of modulating autophagy in pathological cardiac hypertrophy. Biomedicine & Pharmacotherapy, 156, 113967. https://doi.org/10.1016/j.biopha.2022.113967

Shimizu, I., & Minamino, T. (2016). Physiological and pathological cardiac hypertrophy. Journal of Molecular and Cellular Cardiology, 97, 245–262. https://doi.org/10.1016/j.yjmcc.2016.06.001

Wang, B. X., Zhou, Y. T., Zhao, Y. P., Cheng, Y., Ren, J., Tan, G. C., & Wang, X. H. (2025). Hypertrophic cardiomyopathy: Mechanisms of pathogenicity. Biomedical and Environmental Sciences, 38(8), 988–1000. https://doi.org/10.3967/bes2025.096

Wang, S. M., Ye, L. F., & Wang, L. H. (2020). Shenmai injection improves energy metabolism in patients with heart failure: A randomized controlled trial. Frontiers in Pharmacology, 11, 459. https://doi.org/10.3389/fphar.2020.00459

Wang, Y., Liu, Q., Kong, Y., Zhong, G., & Wang, D. (2023). Efficacy and safety evaluation of Shenmai injections for dilated cardiomyopathy: A systematic review and meta-analysis of randomised controlled trials. Phytomedicine, 110, 154630. https://doi.org/10.1016/j.phymed.2022.154630

Wu, Y., Li, T., Li, P., Peng, H., Gao, A., Wang, J., Zhu, H., & Wang, X. (2023). Effects of Shenmai injection against chronic heart failure: A meta-analysis and systematic review of preclinical and clinical studies. Frontiers in Pharmacology, 14, 1338975. https://doi.org/10.3389/fphar.2023.1338975

Xu, W., Zhu, F., Zhang, Y., Li, P., & Sheng, Y. (2024). An overview of the treatments for hypertrophic cardiomyopathy. Frontiers in Cardiovascular Medicine, 11, 1387596. https://doi.org/10.3389/fcvm.2024.1387596

Yang, J., Zhao, M., Zeng, T., Ye, L., Gui, Y., & Wang, L. (2024). Shenmai injection improves lipid metabolism in post-myocardial infarction heart failure based on network pharmacology and experimental validation. Heliyon, 10(21), e38648. https://doi.org/10.1016/j.heliyon.2024.e38648

Zhang, S., You, Z. Q., Yang, L., Li, L. L., Wu, Y. P., Gu, L. Q., & Xin, Y. F. (2019). Protective effect of Shenmai injection on doxorubicin-induced cardiotoxicity via regulation of inflammatory mediators. BMC Complementary and Alternative Medicine, 19(1), 317. https://doi.org/10.1186/s12906-019-2686-2

Zhao, Y., Zhang, F., Zhao, X., Yuan, W., Zhang, J., & Wang, Y. (2018). [Shenmai injection protects mitochondria from oxidative injury in myocardial cells and its mechanism]. Zhejiang Da Xue Xue Bao Yi Xue Ban, 47(5), 507–513. https://doi.org/10.3785/j.issn.1008-9292.2018.10.10

Cite this article: Zhou X, Xu X, Hou X, Wang M, Liang T, Shen P, *et al*. Shenmai Injection Attenuates Pressure Overload-Induced Cardiac Hypertrophy by Modulating HRAS. Pharmacog Res. 2027;19(1):356-69.